SCALAR DISPERSION IN TURBULENT OPEN CHANNEL FLOWS OVER SMOOTH AND ROUGH BEDS

A Thesis
Presented to
The Academic Faculty

by

Zhuo Chen

In Partial Fulfillment
of the Requirements for the Degree
Master of Science in the
School of Civil and Environmental Engineering

Georgia Institute of Technology
August 2012

SCALAR DISPERSION IN TURBULENT OPEN CHANNEL FLOWS OVER SMOOTH AND ROUGH BEDS

Approved by:

Dr. Thorsten Stoesser, Advisor
School of Civil and Environmental Engineering
Georgia Institute of Technology

Dr. Philip Roberts
School of Civil and Environmental Engineering
Georgia Institute of Technology

Dr. Donald Webster
School of Civil and Environmental Engineering
Georgia Institute of Technology

Date Approved: 07/02/2012

To my family and friends

ACKNOWLEDGEMENTS

First and foremost I offer my sincerest gratitude to my supervisor, Dr. Thorsten Stoesser, who has supported me throughout my thesis with his patience and knowledge whilst allowing me the room to work in my own way. I attribute the level of my Master degree to his encouragement and effort, and without him this thesis, too, would not have been completed or written. I would also like express my gratitude to Dr. Donald Webster and Dr. Philip Roberts for their valuable time and effort in serving on my committee.

I also like to thank my lab mates, Sandeep Bomminayuni, Dongjin Kim, Sujin Kim, Sibel Kara and Mustafa Kara for their help and cooperation during my entire stay. And many thanks to my friends at Georgia Tech for making my life here nothing less than wonderful.

Finally, I wish to thank my lovely and caring parents. They were always supporting me and encouraging me with their best wishes.

TABLE OF CONTENTS

LIST OF TABLES

LIST OF FIGURES

SUMMARY

Study of passive dispersion of a neutral scalar in turbulent flows is highly important due to its numerous applications in the areas of turbulent flow visualization, turbulent heat transfer and transport of pollutants and other substances in the environment. Over the past few decades, many analytical, numerical, and experimental studies have been conducted on this topic to obtain a better understanding of the physical process. In the present work, Large Eddy Simulations (LES) of scalar dispersion in turbulent flow over smooth and rough channels is conducted to contribute to the further understanding of the relation between the turbulent velocity field and the concentration field.

The LES results from the present work showed good agreement with a recently completed experimental study(Rahman and Webster [2005]). An in-depth comparison of instantaneous concentration and velocity fields revealed the correlation between scalar dispersion and coherent structures of the turbulent flow. Also, a three dimensional visualization of concentration iso-surfaces at different instants provided a good picture of the concentration structures transported as a result of hairpin vortices of turbulent flow, which is quite difficult to accomplish using experimental studies.

CHAPTER I

INTRODUCTION

The behavior of passive scalars has attracted great interest in the past decades because of its importance in combustion, pollution ,and turbulent mixing. For example, turbulence provides efficient mixing when two chemicals are introduced into a flow to react at the molecular level. And an estimation of toxicological impact from contaminant released by urban population and industrial activities in large urban field is very necessary. Also, it provides impetus to the study of turbulent flow, since the subject of flow visualization depends on interpreting how a passive scalar is related to the velocity field.

The passive scalar, as defined in Warhaft [2000], is a diffusive contaminant in a fluid flow that is present in such low concentration that it has no dynamical effect on the fluid motion itself. The framework to predict the average concentration values has been provided by Fischer et al. [1979], based on a eddy diffusivity model. However, as turbulent eddies are stretching and folding a scalar field, the concentration fluctuation can be even significantly greater than the predicted average concentration. Since the fluctuations occur with spatio-temporal bursts, the velocity field exhibits small-scale intermittency. The connection between intermittency and Navier-Stokes equation is uncertain, and the scalar intermittency occurs in the absence of velocity intermittency as long as there is a multiplicity of scales. They make the study of passive scalar in

turbulent flow even more interesting.

A large variety of research on scalar dispersion in turbulent flows has been undertaken since then 1960s. In the early works, great efforts were made on statistical characteristics of the scalar in simple turbulent flows. For example, Pope [1976], Kollmann and Janicka [1982], Yoshizawa [1988], Sinai and Yakhot [1989], Jayesh and Warhaft [1992], Pope and Ching [1993], Ching [1993], Lane et al. [1993], Shraiman and Siggia [2000], Bakosi et al. [2007] studied probability density function (pdf) of passive scalar. The pdf, which contains information on all the statistical moments, is a very important function in statistical mechanics of turbulence. Pope [1976] derived a time-dependent equation for the probability density of the scalar. Sinai and Yakhot [1989] and Ching [1993] analyzed the Pope's transport equation in a general form and constructed closed-form solutions for the probability density function of passive scalar. Pope and Ching [1993] obtained exact expressions for the pdf in stationary process in different turbulent states. Kollmann and Janicka [1982] discussed first for probability density functions represented as the sum of continuous and singular contribution and pointed out the closure of transport equation depends on closure assumptions for turbulent flux and scalar dissipation term. Jayesh and Warhaft [1992] studied fluctuation of passive temperature experimentally, in respect of the assumption that scalar fluctuations are purely Gaussian. However, they found that the pdf of temperature fluctuation has exponential tails for flow with the Reynolds number greater than 70, and the pdf is close to Gaussian only with a lower Reynolds number. Jayesh and Warhaft [1992]'s results were used as a validation of Ching [1993]'s exact solution. Another compelling area is energy spectra of a passive scalar. Kolmogorov (1941)

developed a model on the base of Richardson's concept of energy cascade to examine the small-scale behavior of the turbulent velocity field. Then this model was applied to a passive scalar field by Obukhov (1949) and Corrsin (1951). The model is based on the local isotropy assumption, and indicates specific functional forms of the velocity and passive scalar structure functions. So works about spectrum function were on the base of applications and extensions of Obukhov's model (Kerstein [1991], Zhu et al. [1995], Sreenivasan [1996], Mydlarski and Warhaft [1998]). Zhu et al. [1995] presented a refined similarity hypothesis of Kolmogorov's theory, considering the fluctuating nature of the dissipation rate. They applied the hypothesis into atmospheric surface layer and a circular jet and found the constants for the second-order velocity and temperature structure functions are in close agreement with classical Kolmogorov's theory. Mydlarski and Warhaft [1998] pointed out that the local isotropy hypothesis is not valid with high *Péclet* number, where different boundary conditions were applied for scalar and velocity fields. But the scalar spectrum is close to 5/3 only if the requirement of an isotropic velocity field is met.

As computer power is growing, numerical simulations of scalar dispersion (Kasagi et al. [1992], Lu and Hetsroni [1995], Overholt and Pope [1996], Nagaosa [1999], Na and Hanratty [2000], Tiselj et al. [2001], Walton and Cheng [2002], Barlow and Belcher [2002], Haverd et al. [2010], Orlandi and Leonardi [2004], Dimotakis [2005], Belcher [2005], Rossi and Iaccarino [2009], Branford et al. [2011], Michioka et al. [2011]) have been booming since the 1990s. Since numerical simulations can provide quantitative data that cannot be obtained experimentally, a better understanding of the transport mechanism has been promoted. Kasagi et al. [1992] carried out a

DNS of the fully developed thermal field in 2D turbulent channel. Temperature was considered as a passive scalar with any buoyancy effect neglected. They obtained root-mean-square temperature fluctuations θ', and found that θ' is closely correlated with the streamwise velocity fluctuation u', particularly in the near-wall region, and the distributions of budget terms for the streamwise and wall-normal heat fluxes $\overline{u'\theta'}$ and $\overline{v'\theta'}$ were very similar to those for the two Reynolds stress components, $\overline{u'u'}$ and $\overline{u'v'}$. Overholt and Pope [1996] revealed that the scalar dissipation depends on Reynolds number, which was concluded from the mechanical dissipation. Also, contours of the scalar through the region of highest scalar gradient magnitude suggested an effect that persists throughout since the highest gradients were close to parallel to spanwise direction. Na and Hanratty [2000] found that the fluctuations in temperature were more damped at high wavenumbers, which happened close to the walls.

Since many engineering and natural environments possess rough surfaces, it's very important to understand the scalar transport over complex terrains.

Mean concentration, concentration fluctuation were discussed in these works, as well as other features that may influence the dispersion process, such as the effect of source height, flow direction, and scalar emission rate. Orlandi and Leonardi [2004] showed that the instantaneous contours of concentration fluctuation is superimposed to velocity vectors with DNS of a passive scalar in complex turbulent rough flows without dealing with the geometric complexity. Xie et al. [2007] compared the transport phenomena of scalars released from an elevated source (ES) and a ground-level source (GLS). They confirmed that relative intensity Γ_0/C_m approaches a constant value downstream, where Γ_0 is the predicted maximum concentration and C_m is

the local mean concentration by large eddy simulation and experiment. Also they observed that the frequency slope approximates -1 in the spectra for GLS and -0.7 for ES. Neither of these spectra showed a clear $-\frac{5}{3}$ region. Wang et al. [2009] discussed the turbulent scalar flux model by comparing result from Reynolds-Averaged Navier-Stokes method (RANS) and experiment. They suggested that set of closure coefficients for concentration variance should be different with that for mean concentration. Branford et al. [2011] found that topological dispersion, which means that small turbulent fluctuations result in large deviation around roughness elements, arises in staggered arranged roughness elements. Also, the geometry in close vicinity of source can influence the secondary source and the near-field concentration distribution. In Rahman and Webster [2005]'s work, an experiment to study the influence of bed roughness on a scalar plume was carried out. Mean and instantaneous properties of velocity and scalar fields were measured. The mean concentrations along the plume centerline is decreasing as a power law $x^{-1.5}$ close to the source and x^{-1} downstream of the source. The plume width increased in proportion to $x^{0.75}$ near the source and $x^{0.5}$ farther downstream. A conclusion that the scalar variance decreases as a power law $\tilde{c}^2 \propto (x/H)^{-n}$, where $n = 3.5$ for region close to source and $n = 4.5$ downstream was drawn. Also, the concentration fluctuation intensity decreases faster with a rougher bed.

Over the past two decades, various experimental and numerical investigations have been conducted on scalar dispersion in turbulent flow over rough surfaces. However, a universal and accurate statistical description of scalar dispersion is not yet available. One of the reasons is the geometry and size of roughness elements and the effective

Table 1: Geometry of roughness elements in recent works

Paper	Type	Roughness Element	$D/k^{(1)}$
Barlow and Belcher [2002]	EXP[2]	Mesh	-
Xie et al. [2007]	LES, EXP	Cube	120
Haverd et al. [2010]	EPX	Globe and trunk	21
Michioka et al. [2011]	LES	Transverse bar	14.2
Orlandi and Leonardi [2008]	DNS	Cubes and Wedges	-
Branford et al. [2011]	DNS	Cubes	32, 64

[1] The channel depth is assumed as boundary layer depth in boundary-layer flow.

[2] EXP: experiment, LES: large eddy simulation, DNS: direct numerical simulation

position of the bed. Generally, the equivalent sand-roughness height K_s is used to characterize roughness elements. The definition of K_s will be further explained in the next chapters. But the effects of different roughness elements' geometries is very significant, and it'll be discussed by comparing numerical and experimental results. Future study is required in order to quantify the effects. In Table. 1, the geometry of roughness elements in recent papers is displayed.

Moreover, some researchers have focused on scalar dispersion mechanism and correlation between scalar dispersion and turbulent structures. In Grass [1971]'s experiment on rough wall flows, turbulent coherent structures were observed similar to those over a smooth wall. He suggested that the ejection and inrush events contribute to energy dissipation and turbulence production. Grass et al. [1991] and Defina [1996] confirmed these findings and also provided insights on the variation of transverse streak spacing across the channel depth. Kim and Moin observed that in the near wall region, the scalar was distributed in high- and low-speed region. Negative fluctuations occurred in the high and positive in the low-speed regions. Orlandi and Leonardi [2004] examined in detail how the passive scalar structures are linked to the

velocity structures. They extended Kim and Moin's analysis to a higher Re number and without constant heat source. The mechanism of heat losses at the wall was due to the action of the molecular diffusivity in the very near wall region; then the scalar was transported far from the wall by the velocity fluctuations. Babiano and Provenzale [2007] observed that enstrophy and passive-tracer variance undergo different inertial-range cascade processes in elliptic regions, where enstrophy dominates.

In this present study, LES of turbulent flow and scalar transport is performed over a smooth channel bed and a channel bed artificially roughened by cubes placed in a staggered array. Based on the data from the simulation, the first and second order turbulent statistics are compared with published experimental results, and coherent structures in the flow are also identified and quantified. The results are found to be consistent and in good agreement with the experiments. Also, the effect of turbulence structures on scalar transport is investigated. Therefore, the major objectives of the present numerical study using Large Eddy Simulation (LES) are to :

(1) Understand the effects of roughness on the flow properties and quantify coherent structures in the flow.

(2) Provide three-dimensional plots of the concentration structures together with turbulent coherent structures, especially in the near-bed region.

(3) Correlate the dynamic process of scalar dispersion over smooth and rough beds.

The thesis is organized into five chapters. The following chapter presents the numerical framework. The third shows the validation of smooth and rough turbulent flows and chapter four reports on the results of scalar dispersion in turbulent flows

over smooth and rough beds. Finally, the last chapter contains the conclusions and some suggestions for future work.

CHAPTER II

NUMERICAL FRAMEWORK

2.1 Large Eddy Simulation

Modeling of any fluid flow problem involves identification of governing equation and application of numerical methods for solving those equations. The choice of equations and numerical methods decides the computational time and accuracy of solutions. This chapter will discuss in detail the modeling applied in our study of scalar dispersion in turbulent flows over smooth and rough beds.

The Navier-Stokes equations, named after Claude-Louis Navier and George Gabriel Stokes, describe the motion of fluid. In case of an incompressible fluid, such as water, the continuity equation needs to be solved as well. Three approaches are generally applied into solving these equations: Reynolds Averaged Navier-Stokes simulation (RANS), Large Eddy Simulation (LES) and Direct Numerical Simulation (DNS).

One of the key challenges in turbulence research is to understand relationships between the structure, dynamics, and statistics of small and large scales of motion. In high Reynolds number applications, direct-numerical simulations (DNS) of turbulence is generally impossible, because of the wide range that exists between largest and smallest dissipative scales which cannot be explicitly simulated even on the powerful computers. Since the large scales of flow attracts more interest since they control

turbulent diffusion of momentum and heat. Simulations using the large-eddy simulation(LES) approach could be an useful alternative. In the large-eddy simulation(LES) approach, one gets rid of the scales of wavelength smaller than the grid mesh Δx by applying an appropriately chosen low-pass filter characterized by the function $\bar{G}$ to the flow to eliminate the fluctuations on subgrid scales. The filtered field is defined, for any quantity f(scalar or vectorial),as

$$\bar{f}(\mathbf{x},t) = \int f(\mathbf{y},t)\bar{G}(\mathbf{x}-\mathbf{y})d\mathbf{y} = \int f(\mathbf{x}-\mathbf{y},t)\bar{G}(\mathbf{y})d\mathbf{y} \tag{1}$$

Here the filter $\bar{G}$ is independent of the position $\mathbf{x}$, which simplifies much of the formalism(Lesieur and Metais [1996]). One can easily check that the fileter defined by Eq. 1 commutes with temporal and spatial derivatives, so that the continuity equation

$$\frac{\partial \bar{u_j}}{\partial x_j} = 0 \tag{2}$$

holds for the filtered field. One considers the Navier-Stokes equations in the form:

$$\frac{\partial u_i}{\partial t} + \frac{\partial}{\partial x_j}(u_i u_j) = -\frac{1}{\rho_0}\frac{\partial p}{\partial x_i} + \frac{\partial}{\partial x_j}[\nu(\frac{\partial u_i}{\partial u_j} + \frac{\partial u_j}{\partial u_i})] \tag{3}$$

. After applying the filter, one gets

$$\frac{\partial \bar{u}_i}{\partial t} + \frac{\partial}{\partial x_j}(\bar{u}_i \bar{u}_j) = -\frac{1}{\rho_0}\frac{\partial \bar{p}}{\partial x_i} + \frac{\partial}{\partial x_j}[\nu(\frac{\partial \bar{u}_i}{\partial x_j} + \frac{\partial \bar{u}_j}{\partial x_i}) + T_{ij}] \tag{4}$$

where the subgrid-scale tensor T_{ij} is given by $T_{ij} = \bar{u_i}\bar{u_j} - u_i\bar{u}_j$.

The passive scalar convected by the flow satisfies

$$\frac{\partial C}{\partial t} + \frac{\partial}{\partial x_j}(C u_j) = \frac{\partial}{\partial x_j}(\kappa \frac{\partial C}{\partial x_j}) \tag{5}$$

. If the filter $\tilde{G}$ is applied to this equation, one finds

$$\frac{\partial \bar{C}}{\partial t} + \frac{\partial}{\partial x_j}(\bar{C}\bar{u}_j) = \frac{\partial}{\partial x_j}(\kappa \frac{\partial \bar{C}}{\partial x_j} + \bar{C}\bar{u}_j - C\bar{u}_j) \tag{6}$$

. The last two terms are modeled with an eddy diffusivity κ_t to yield

$$\frac{\partial \bar{C}}{\partial t} + \bar{u}_j \frac{\partial \bar{C}}{\partial x_j} = \frac{\partial}{\partial x_j}[(\kappa + \kappa_t)\frac{\partial \bar{C}}{\partial x_j}] \tag{7}$$

The turbulent Prandtl number is defined as $Pr^t = \nu_t/\kappa_t$.

Large-eddy simulations have been shown in the past decades to predict remarkably well the mean properties of turbulent flows of moderate complication. In this present study, the large-eddy simulation approach using LES source code, Hydro3D (Stoesser,2002) is employed. This code is based on the finite volume method on a Cartesian grid with collocated variable arrangement.

2.2 Governing Equations and Numerical Method

The filtered continuity and Navier-Stokes equations are as follows (Pope,2000):

$$\frac{\partial u_i}{\partial x_j} = 0 \tag{8}$$

$$\frac{\partial u_i}{\partial t} + \frac{\partial u_i u_j}{\partial t} = -\frac{\partial P}{\partial x_j} + \frac{\partial (2\nu S_{ij})}{\partial x_j} - \frac{\partial \tau_{ij}}{\partial x_j} \tag{9}$$

where u_i and $u_j (i \text{ or } j = 1, 2, or 3)$ = resolved velocity vectors; and p is resolved pressure divided by the density. These equations are filtered in space. Similarly, x_i and x_j represent the spatial location vectors in x,y, and z axis direction, respectively. ν is kinematic viscosity ; and S_{ij} is filtered strain-rate tensor, which is defined as

$$S_{ij} = \frac{1}{2}(\frac{\partial u_i}{\partial x_j} + \frac{\partial u_i}{\partial x_j}) \tag{10}$$

the term τ_{ij} results from the unsolved sub-grid scale fluctuations and must be modeled by a sub-grid scale model. The dynamic version of the original Smagorinsky (Smagorinsky,1963) sub-grid scale (SGS) model (Germano et al. [1991]) is employed to approximate the anisotropic part of τ_{ij}, i.e. τ^a_{ij}, as $\tau^a_{ij} = \tau_{ij} - \frac{2}{3}\delta k_r (= -2\nu_t S_{ij})$, where δ_{ij} is the Kronecker delta and k_r is the residual kinetic energy. Then an anisotropic filter ($\Delta = (\Delta x \Delta y \Delta z)^{1/3}$) together with the characteristic filtered rate of strain ($|S| = (2S_{ij}S_{ij})$) are used to ocmpute the sub-grid scale eddy viscosity ν_t as $\nu_t = (C_s\Delta)^2|S|$. The Smagorinsky constant C_s is calculated locally by making use of the flow information available from the smallest resolved scales. A double filtering procedure leads to a closed expression, commonly referred to as Germano's identify, relating filter stresses at different filter levels to each other. This additional information is then used to determine the model parameter C_s through local averaging.

A Poisson equation is solved iteratively for coupling the pressure to velocity field using the SIP method of Stone (1968). The convection and diffusion terms in the Navier-Stokes equations are approximated by central differences ensuring second-order accuracy in space. The convection term in Eq. 11 is computed using the HLPA scheme proposed by Zhu(1991) An explicit Runge-Kutta scheme is used to discretize the equations in time providing second-order accuracy in time.

Transport of a conservative tracer was simulated in the LES by solving the following three-dimension advection-diffusion equation for the filtered tracer concentration(Kim et al. [2010]), C:

$$\frac{\partial C}{\partial t} + u_j \frac{\partial C}{\partial x_j} = D_t \frac{\partial^2 C}{\partial x_j^2} \tag{11}$$

where C is the resolved concentration, $D_t = \nu_t/Sc_t + \nu/Sc$. ν_t is the subgrid-scale eddy viscosity, and Sc_t is turbulent Schmidt number. The turbulent Schmidt number in the LES was set to 1000 to maintain the same ratio of molecular viscosity of water to the molecular viscosity of the tracer used in the experiments by Rahman and Webster [2005].

CHAPTER III

VALIDATION OF TURBULENT FLOWS OVER SMOOTH AND ROUGH BEDS

Many researchers, for example, Bhaganagar et al. [2004], Leonardi et al. [2006], Orlandi and Leonardi [2008] and Bomminayuni and Stoesser [2011] have conducted DNS or Large-eddy simulation of flows over smooth and rough beds. The simulation results were generally found to be in good agreement with experiments, data of which served as a validation for their models. The following sections in this chapter present the validation of flow over smooth and rough bed large-eddy simulations performed using the Hydro3d code.

3.1 Setup and Boundary Conditions

The simulation setup of this study was chosen to match the experiments carried out by Rahman and Webster [2005]. They carried out measurements of velocity and scalar dispersion was studies over a smooth bed and three types of rough beds. The computational domain of the simulations had dimensions of $8H$ in streamwise and $4H$ in spanwise direction, with H being the depth of the flow. In the present work, the roughness treatment was simplified as cubical elements, located at the bottom of the domain. In the present coordinate system, x and y directions are defined as streamwise and spanwise coordinates respectively, and z is the vertical direction coordinate with $z = 0$ at the bottom of domain for smooth case and at the top of

the equivalent roughness height for the rough case. The Reynolds number of the flow based on channel flow depth (H) is equal to 10000. The Schmidt number in the LES is 0.7, which was suggested in Launder [1978]. This is considered as a standard value and is also used in commercial codes as a default value. Periodic boundary conditions were applied in spanwise and streamwise directions, assuming a homogeneous turbulent flow in both two directions. At the channel bed and on the surface of the cubes a no-slip boundary condition was applied. The free surface was treated as a plane of symmetry with zero shear. The initial flow field was uniform but with random perturbations. The flow was in statistically steady state when the turbulence was fully developed, which was after approximately 20 flow through times. For the rough bed flow simulation, the channel bottom roughness is represented by cubical elements, placed in a staggered arrangement. The distance between two neighboring cubes is $0.5H$, and the characteristic dimensions of the cube are as follows: $X_c/H = 0.1, Y_c/H = 0.1, Z_c/H = 0.1$. The setup along with boundary conditions and roughness element distribution is shown in Fig. 1.

The computational grids used in the simulation is of high resolution and consisted of 801×401 numerical points equally spaced in x, y direction, respectively. In z direction, the grid was uniform below $0.2H$, consisted of 40 cells. The grid was stretched towards the water surface in the upper region, and consisted of 60 cells. Fig. 2 shows the $x - z$ grid where every fifth grid point is plotted. The grid spacings are shown in Table. 2.

The grid in LES acts as a filter which separates large-scale eddies from small-scale eddies. Hence, in the LES, the grid is required to be fine enough so that the simulation

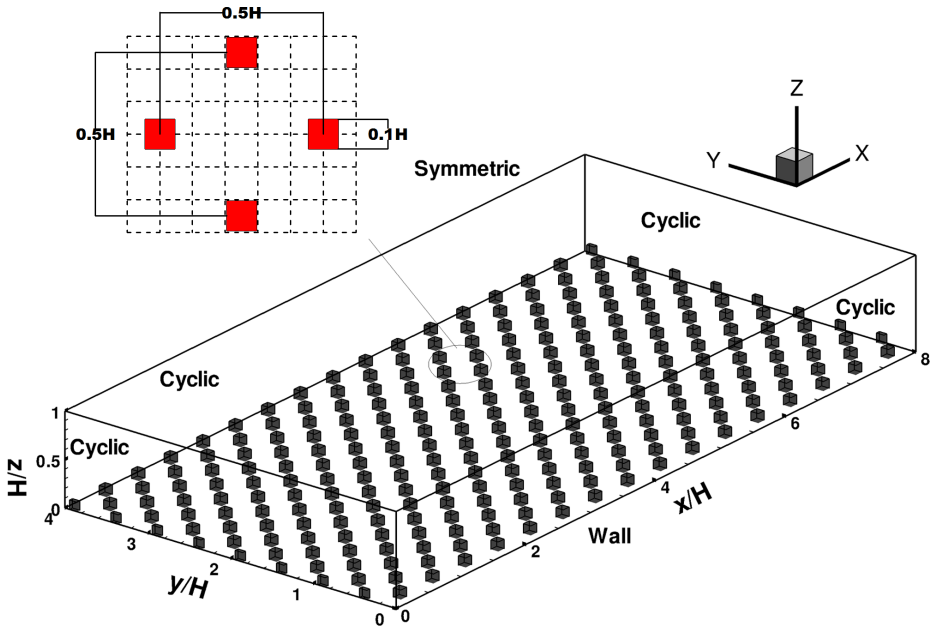

Figure 1: Setup and boundary conditions

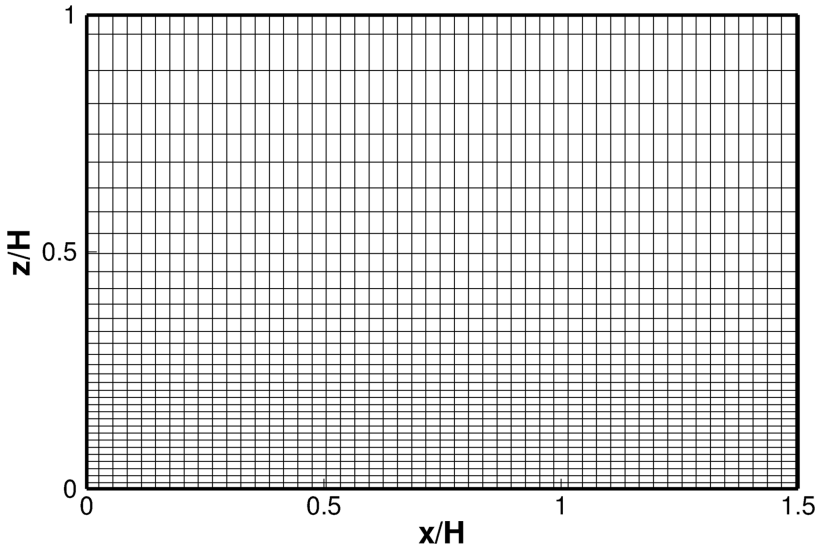

Figure 2: Computational grid in a cross-section

Table 2: Grid Spacing in Smooth and Rough Cases

Case	Re	Re_τ^1	$N_x \times N_y \times N_z^2$	$\Delta x^+ \Delta y^+ \Delta z^+_{min}$	Δz^+_{max}
Smooth	10000	553	$800 \times 400 \times 100$	$5.53 \times 5.53 \times 2.77$	15.15
Rough	10000	1120	$800 \times 400 \times 100$	$11.2 \times 11.2 \times 5.6$	30.69

[1] $Re_\tau = Hu^*/\nu$

[2] N_x, N_y, N_z are the numbers of cells of domain in x-,y-,and z-directions.

[3] $\Delta x^+ = \Delta x u^*/\nu$, Δy^+ and Δz^+ are similar.

(a) properly captures the largest eddies in the production range of the energy spectra and (2) cascades these eddies within the inertial subrange in a physically realistic way. It was found that the grid captured the production range and provided a wide range of captured turbulent scales.

3.2 Statistics of Turbulent Flows

A quantitative comparison of the simulation results with experimental data was performed to validate the simulation. As a validation of the flow, mean and root mean square (rms) of the streamwise velocity, and Reynolds shear stress are compared against experimental results of Rahman and Webster [2005].

Fig. 3 shows the time and spatially averaged smooth and rough channel LES streamwise velocity profiles along with those of Rahman and Webster [2005]. Since the exact value of boundary layer thickness used in the rough case was unknown, it is necessary to develop functional relationships between the roughness geometry and its influence on mean flow characteristics. In the present work, the equivalent sand roughness (k_s) and the effective location of the bed (δ) were estimated by a best-fit procedure (Bomminayuni and Stoesser [2011]), which yielded $k_s = 0.80k$ and $\delta = 0.2k$,where k is the height of roughness element. The best fit procedure employed here could be described as follows. First, the LES velocity profile was plotted for different δ values to have the same slope as the log-law velocity profile over a smooth bed. Then the downward shift ΔB was calculated as the average distance between the LES profile and the smooth channel log-law velocity profile. This was done for the region $50 < z^+ < 500$, where z^+ was defined as the vertical distance from the

effective bed location in viscous units(i.e. $z^+ = zu_*/\nu$). From the so obtained ΔB the equivalent sand-grain roughness k_s was calculated directly using the formulation given by Schlichting (1965):

$$\Delta B = B - 8.5 + \frac{1}{\kappa} \ln k_s^+ \tag{12}$$

where $B = 5.2$ is an empirical constant; and $\kappa =$ is the von Karman constant with $\kappa = 0.41$. The formulation yielded a roughness Reynolds number k_s^+, defined as $k_s^+ = k_s u_*/\nu$, of 253, which was greater than 70 and thus indicated a fully rough turbulent flow regime.

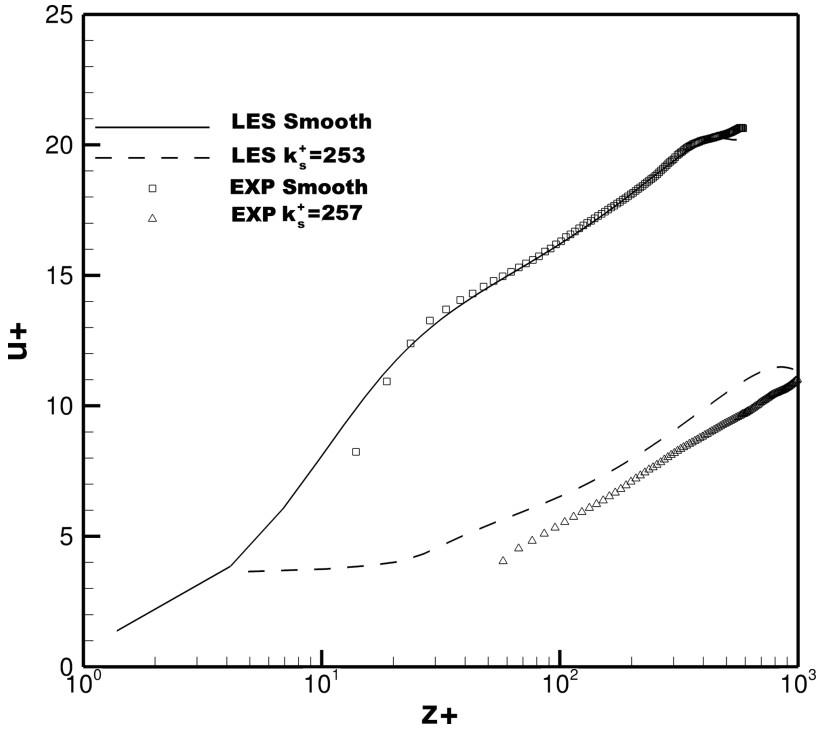

Figure 3: Comparison of mean streamwise velocity profiles from LES with previous experimental study. Here, $u^+ = u/u^*$,$z^+ = zu^*/\nu$

In Fig. 3, the y-axis variable u^+ is the normalized spatially averaged velocity($u^+ = u/u_*$). The dotted line represents the corresponding log-law velocity profile in Rahman and Webster [2005]'s results. The rough-channel LES profile exhibits a downshift

from the smooth-channel profile, revealing that an increase in roughness Reynolds number, i.e., k_s^+ leads to an increased downshift in the mean velocity profile. The smooth wall results are in good agreement with the experimental data. In the rough case, the absence of viscous sublayer is clearly observed, which is due to the penetration of the roughness elements into the logarithmic region.

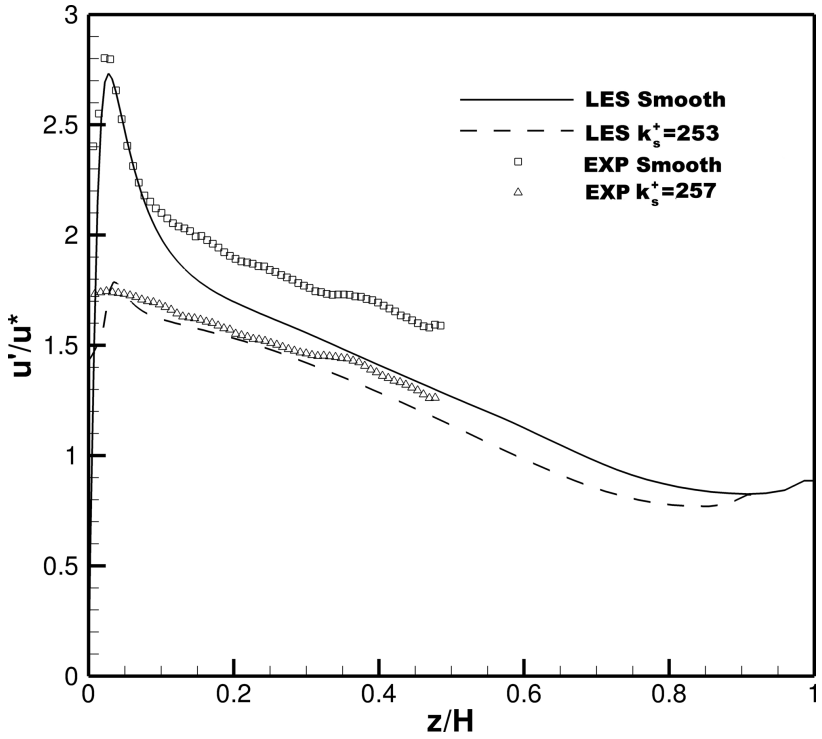

Figure 4: Comparison of normalized streamwise turbulent intensities u'/u^* from LES with experiment

The vertical distribution of streamwise turbulent intensity (u'/u_*) is presented in Fig. 4. u' represents the rms fluctuation of streamwise velocity. The figure plots LES results against data of Rahman and Webster [2005]. It can be observed that the overall agreement is fairly good, in particular there is a good match of peak turbulence intensity. There is a distinct peak in the profile of streamwise turbulent intensity in the smooth channel. While in the rough channel, the profile of streamwise turbulent

intensity is more even. It can be explained as the absence of viscous sublayer. The comparison of smooth and rough channel data suggests the influence of bed roughness on the streamwise turbulent intensity over the entire channel depth.

Fig. 5 shows the Reynolds shear stress (normalized by the square of the shear velocity) variation ($< u'w' > /u_*^2$) in the wall-normal direction. The solid and dash lines correspond to results from LES of smooth and rough cases, and the symbols correspond to experimental results of Rahman and Webster [2005]. The peaks in Reynolds shear stress occur at regions close to the bed, indicating the high rates of momentum transfer. The overall agreement is quite good for smooth case, but the rough case exhibits some difference in magnitude.

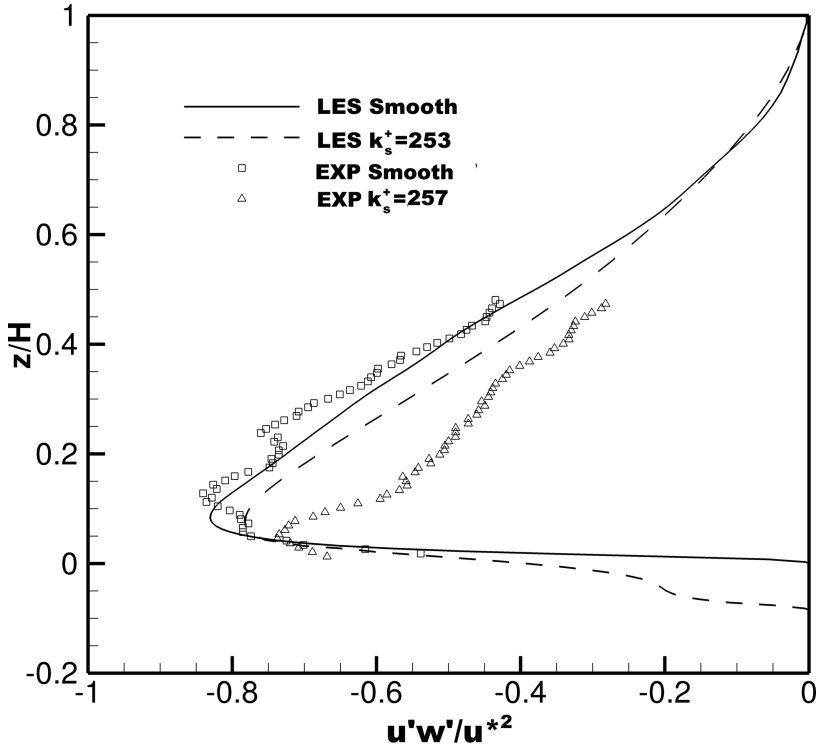

Figure 5: Comparison of normalized spatial-averaged Reynolds shear stress $u'w'/u*^2$ from LES with experiment

3.3 Eduction of Turbulent Flows

Visualization of the turbulent structure plays an important role in qualitative appreciation of the physical processes. Generally flow regimes, in which associated velocities are unknown, are detected by flow visualization. In this section, eduction of turbulent flow are presented for a qualitative validation of the simulation, which can not be obtained from the statistics.

Fig. 6 shows the contours of the instantaneous streamwise velocity fields in an x-z plane. Fig. 6(a) is the instantaneous streamwise velocity field for the smooth case. Fig. 6(b) and Fig. 6(c) are instantaneous streamwise velocity field in the valley and over cubes, respectively. The highly turbulent nature of the flow is evident from this figure especially in the near wall region. The instantaneous flow pattern is much more complex than that of the mean flow (compare with Fig. 10). The velocity field is strongly inhomogeneous, and vortical structures are present throughout the flow. The nature of flow is in accordance with flow behavior typically observed in experiments.

Snapshots of the velocity field in a streamwise-vertical (x-z) plane are shown in Fig. 7, Fig. 8 and Fig. 9. In each case, some vectors were skipped to avoid data congestion. A sequence of plots of the instantaneous velocity field as those shown in Fig. 6 and Fig. 7 to Fig. 9 shows that the flow at the simulated Reynolds number is highly unsteady and departs significantly from the mean flow. Also, the fluctuating velocity vectors indicate the occurrence of ejection- and sweep-type events in the flow. Such momentary events are marked with E (for ejection) and S (for sweep). As Fig. 7, Fig. 8 and Fig. 9 show, at the selected instant in time, several sweep (S) and

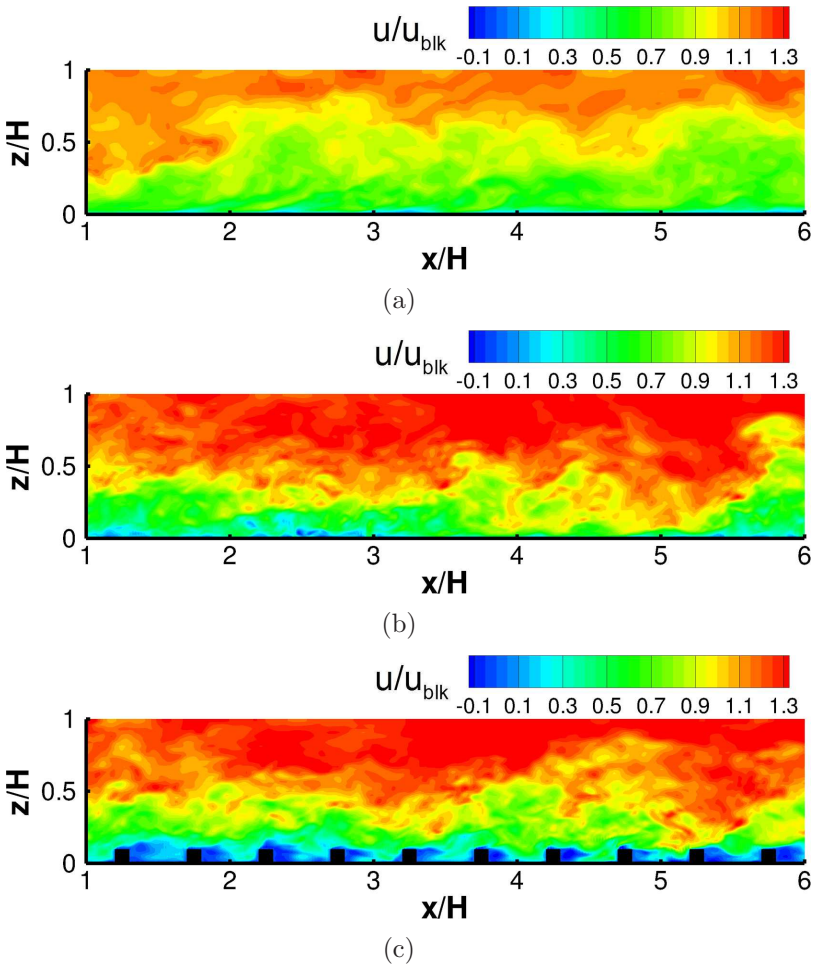

Figure 6: Contours of instantaneous streamwise velocity u/u_{blk} in x-z plane:(a) over the smooth bed (b) in the valley between cubes over rough bed (c) in a plane over cubes

ejection (E) events occur. For example, the low momentum fluid is ejected away from the wall in the area marked as E, and inrushes of high momentum fluid from outer layer occur in the area marked as S. In Fig. 8, above the ejection event, the signature of a hairpin vortex (as HP in the plots) is found, followed by another sweep.

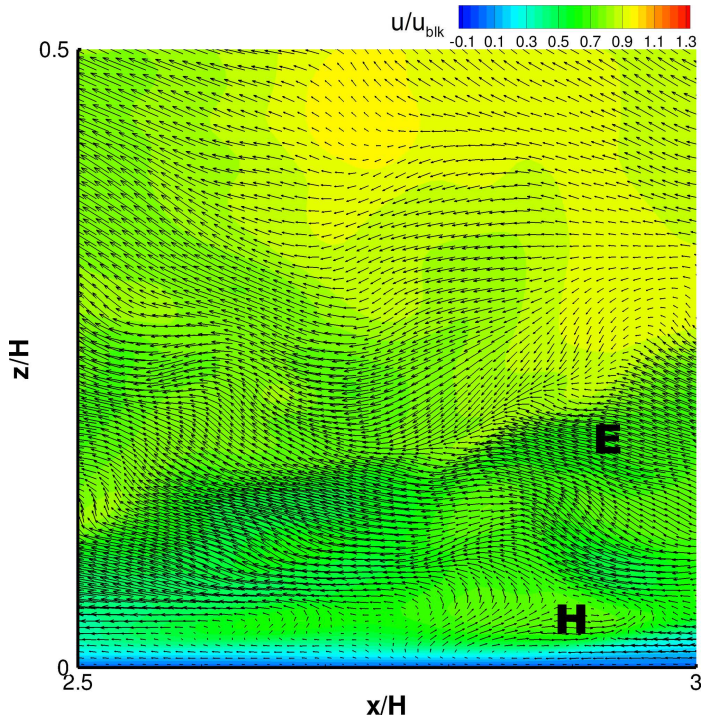

Figure 7: Snapshot of instantaneous velocity fluctuation vectors (u', w') in x-z plane over the smooth bed

Fig. 10 shows time-averaged velocity field plotted similar to Fig. 6 The time-averaged streamwise velocity contours are also plotted in Fig. 10. The boundary layers over the beds are shown clearly. The flow separation occurring around the cubes plays a major role in the generation of near-wall turbulence.

Fig. 11 shows an instantaneous distribution of u' normalized with the shear velocity u^*. The presence of coherent structures of high and low speed streaks alternating in the spanwise direction is visible.

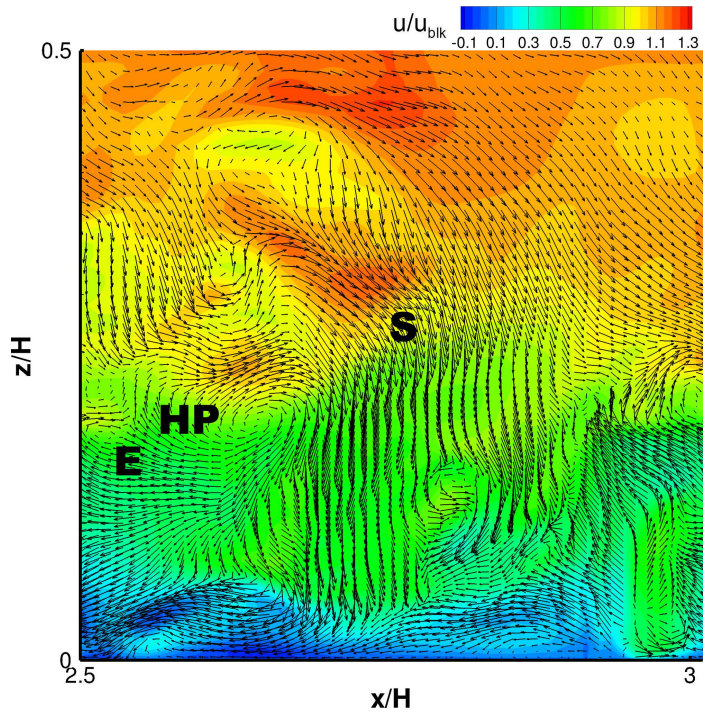

Figure 8: Snapshot of instantaneous velocity fluctuation vectors bed

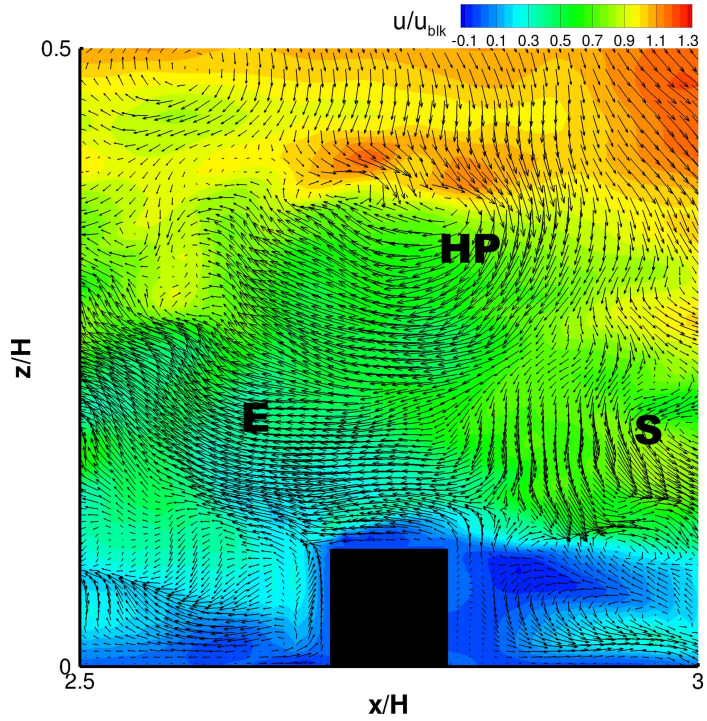

Figure 9: Snapshot of instantaneous velocity fluctuation vectors (u', w') in x-z plane on the slice through cubes over rough bed

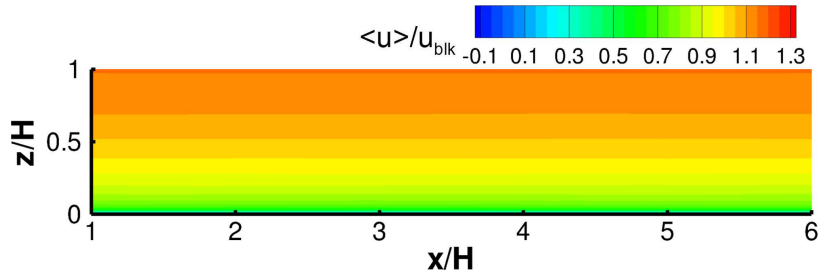

(a)

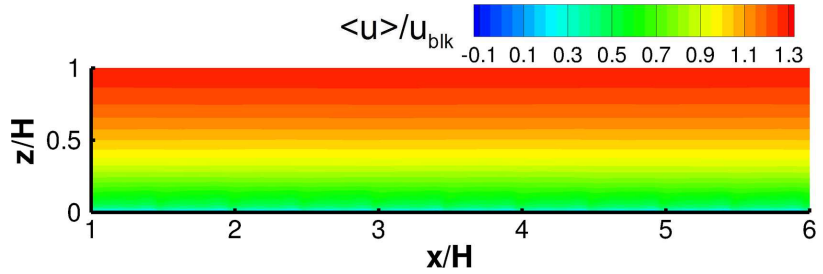

(b)

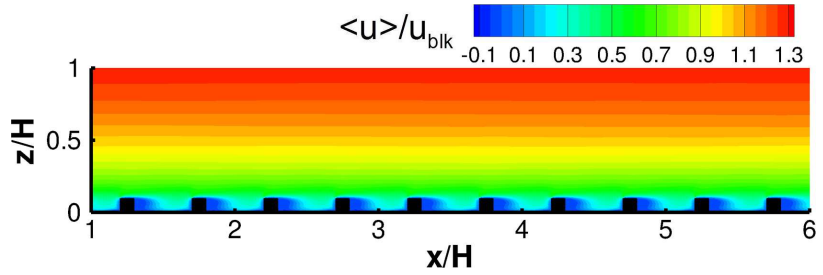

(c)

Figure 10: Contours of time-averaged streamwise velocity $< u > /u_{blk}$ in x-z plane:(a) over the smooth bed (b) in the valley over rough bed (c) on the slice through cubes over rough bed

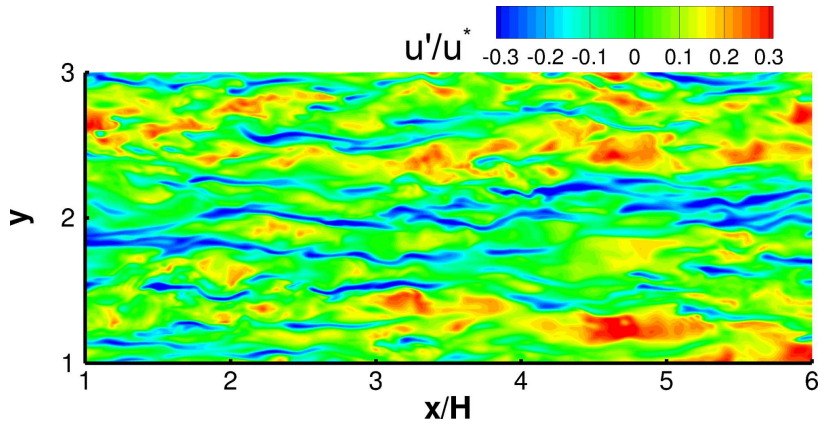

Figure 11: Streak structures on x-y plane over smooth bed

3.4 Conclusion

In this section, the analysis of velocity field from a LES of flow with smooth and rough beds were presented. Comparison with previous experimental and numerical studies were drawn to validate the simulations. It was observed that the results match fairly well with experiments of Rahman and Webster [2005].

CHAPTER IV

SCALAR DISPERSION IN TURBULENT FLOWS OVER SMOOTH AND ROUGH BEDS

Numerous studies have been conducted to date to understand the characteristics of scalar dispersion in turbulent flow. Most of these works reported on mean concentration, concentration fluctuations, instantaneous concentration distribution, probability density function, and spectra of a scalar. However, limited work has been done on three dimensional analysis of the scalar dispersion and the role of turbulence structures in the transport of a scalar. In the following, one to three dimensional views of spatial concentration distributions together with flow structures will be given, which will provide a direct and accurate understanding of the correlation between velocity and concentration fields.

4.1 Statistical Characteristics of a Passive Scalar in a Turbulent Channel Flow

Analyzing the mean concentration field provides insight into the behavior of the passive scalar in space. The analytical framework for an idealized scalar plume, which ignores shear and inhomogeneous diffusivities in the flow, can be used as a baseline for the comparison with numerical results as well as experimental results. The steady-state turbulent transport of a passive scalar in a flow field with mean

velocity $(\overline{u}, 0, 0)$ is given in Crimaldi and Koseff [2006] by

$$\overline{u}\frac{\partial \overline{C}}{\partial x} = \frac{\partial}{\partial y}(D_y \frac{\partial \overline{C}}{\partial y}) + \frac{\partial}{\partial z}(D_z \frac{\partial \overline{C}}{\partial z}) \tag{13}$$

The simple analytical solution is

$$\overline{C}(x, y, z) = \frac{\dot{m}}{4\pi x \sqrt{D_y D_z}} \exp(-\frac{y^2}{2\sigma_y^2} - \frac{z^2}{2\sigma_z^2}) \tag{14}$$

where lateral and vertical concentration profiles are Gaussian with standard deviations

$$\sigma_y = \sqrt{2D_y x/\overline{u}} \tag{15}$$

and

$$\sigma_z = \sqrt{2D_y x/\overline{u}} \tag{16}$$

The lateral mean concentration profiles are self-similar, with the plume size growing proportional to $x^{1/2}$ and magnitudes decaying proportional to x^{-1}.

In the present study, the scalar source was located on the domain centerline. The nozzle was $0.02H$ in width and $0.01H$ in height. The center of the nozzle was located at $0.125H$ above the bottom which corresponds to the experiments of Rahman and Webster [2005]. For the rough bed, the nozzle's elevation was decided by equivalent effective roughness height.

The time-averaged concentration on the centerline of the nozzle is shown in Fig. 12. As the bed turns from smooth into rough, the time-average concentration decreases. For both smooth and rough beds, the average concentration decreases rapidly close to the nozzle. For $x/H < 2.5$, the rate of decrease follows $x^{-1.5}$ for both smooth and rough beds. While for $x/H > 2.5$, the rate of decrease follows x^{-1}. Overall, the slope

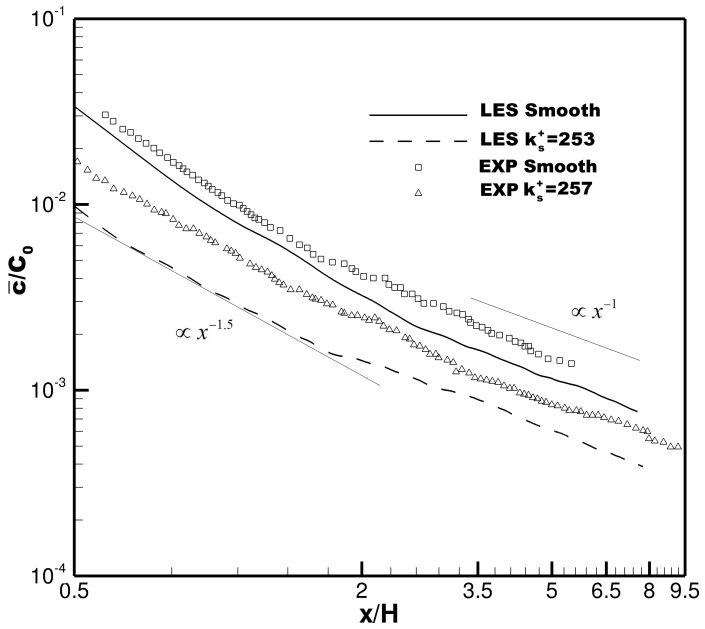

Figure 12: Comparison of mean concentration $\bar{c}/C_0$ on plume centerline from LES with experiment

of concentration distribution is in good agreement with experimental results. The lower magnitude in LES can be because of the higher scalar dispersion observed in the presence of cube. This behavior is observed in Fig. 14.

From Fig. 12, the experimental and numerical results are almost parallel, but the averaged concentration from numerical simulation is always lower than the experimental results, which can be explained as the difference in nozzle areas in two cases. The nozzle in numerical case was square due to the Cartesian grid, while in the experiment it was circular. Also, the wider plume indicates that scalar spreads over wider area in numerical simulation. The present of a cube right in front of the scalar released point may have caused the separation of scalar around the cube leading to a spread of the tracer over a wider area.

Fig. 13 shows the transverse distribution of time-averaged concentration at the

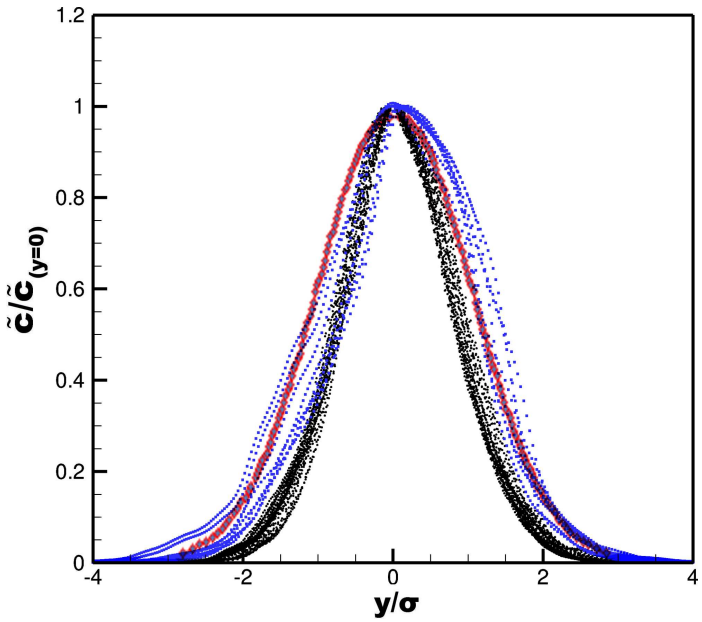

Figure 13: Self-similar transverse profiles of average concentration at selected slices between x/H=2 to 7 (a) Black circle: smooth bed (b) Blue square: rough bed (c) Red line: Gaussian Distribution

height of $0.125H$ at selected slices between x/H=2 to 7. The transverse profiles of average concentration are self-similar and Gaussian for the smooth bed. But for the rough case, the transverse profiles are not exactly symmetric and Gaussian, which could be caused by the asymmetric distribution of roughness elements. However, rough bed profiles spread a wider area. This is in accordance with findings from Rahman and Webster [2005]

Fig. 14 shows the transverse plume width. The plume width is defined as 4σ, where σ is the standard deviation of the Gaussian profile. The transverse profiles follow Gaussian distribution $\overline{c} = \overline{c}_{y=0} \exp(-y^2/2\sigma^2)$, the value of standard deviation is determined from a linear regression between $\ln(\overline{c}/\overline{c}_{y=0})$ and y^2(Rahman and Webster [2005]). The relationship between growth rate of the plume width and the decrease of average concentration along the centerline was discussed in the present work with

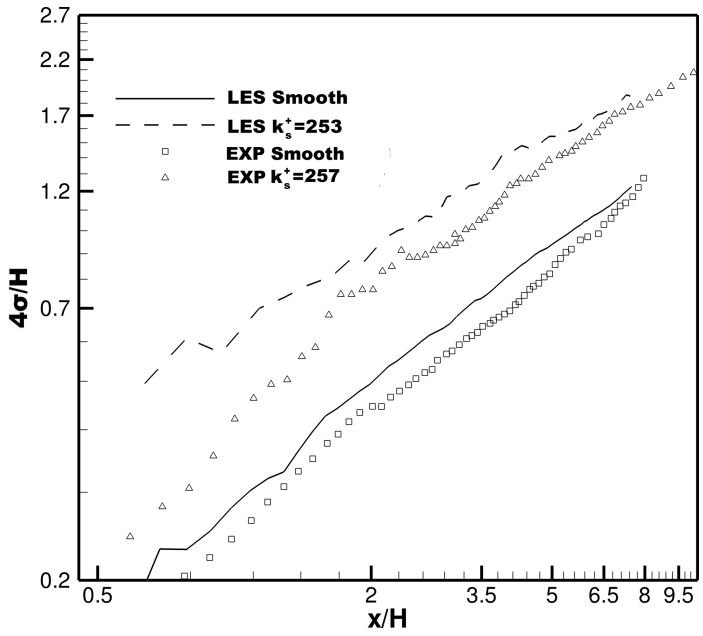

Figure 14: Comparison of transverse plume widths for smooth and rough beds from LES with experiment

Rahman and Webster [2005]'s method. First of all, it is assumed that the analytical solution for the concentration field downstream of a point source in a uniform flow with constant diffusivity is valid(Fischer et.al 1979)

$$\overline{c(x,y,z)} \propto \frac{M}{4\pi\sigma_y\sigma_z} \exp -\frac{y^2}{2\sigma_y^2} - \frac{z^2}{2\sigma_z^2} \tag{17}$$

The plume is assumed to be axisymmetric, which meant $\sigma_y = \sigma z = \sigma$. The standard deviation is assumed to vary as a power law, $\sigma \propto x^p$. So the substitution yield $\overline{c}_{y=0,z=0} \propto x^{-2p}$. The LES results suggest that the plume width increase with $x^{0.76}$ for smooth bed, and $x^{0.57}$ for rough bed along the centerline. As a result, the average concentration decreases close to $x^{-1.5}$ for smooth bed, which is in accordance with Rahman and Webster [2005]'s experimental results. And over rough bed, it is proportional to $x^{-1.1}$, similar with Rahman and Webster [2005]'s x^{-1}.

The plume width from LES is wider in the area close to nozzle than that from

experiment. It is because of the geometry and distribution of roughness element. The heterogeneous roughness elements accelerate the transverse dispersion, leading to a wider plume width and lower concentration on the centerline of the plume.

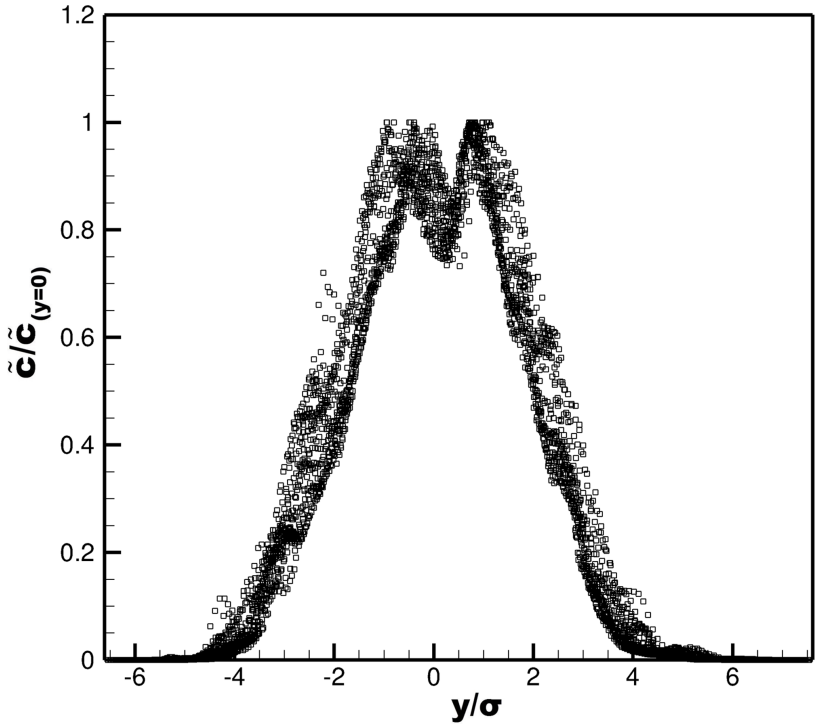

Figure 15: Self-similar transverse profiles of standard deviation of concentration fluctuations at every 0.05 from $x/H = 3$ to 6

Fig. 15 shows transverse profiles of standard deviation with off-centerline peaks for smooth bed. Fig. 16 shows transverse profiles of standard deviation with off-centerline peaks for rough bed. Since concentration and higher-order concentration statistics are significantly influenced by the distribution of roughness elements, two typical locations were chosen to show the transverse profiles of standard deviation for rough bed. The off-axis bipolar maxima has been reported in several previous studies of similar flow(Yee et al. [1993], Rahman and Webster [2005]). Yee et al. [1993] suggested that off-axis maxima occur when the plume spreading is dominated

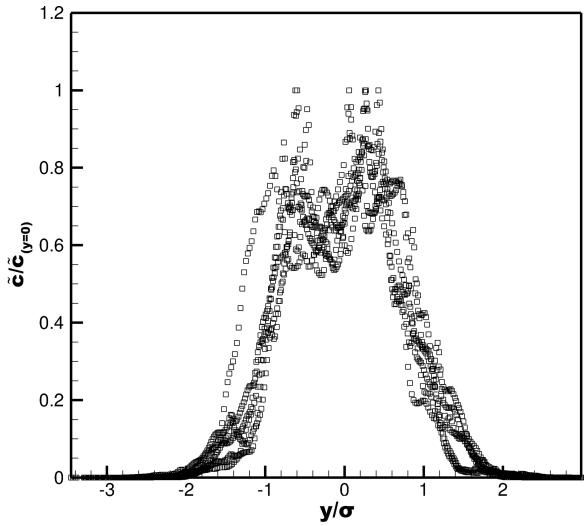

(a)

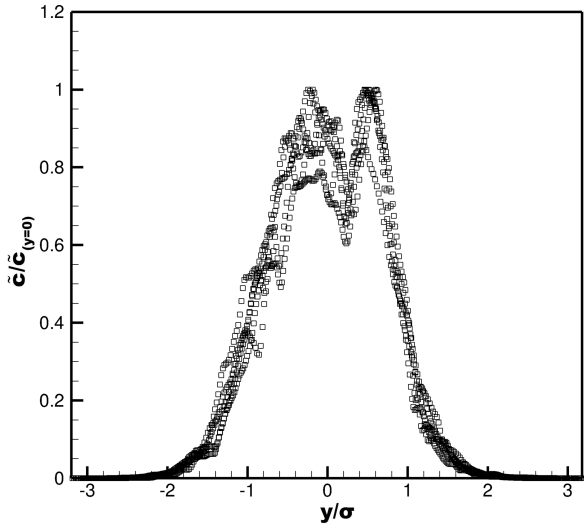

(b)

Figure 16: Self-similar transverse profiles of standard deviation of the concentration fluctuations at different locations with rough bed:(a) x/H=2.75, 3.25, 3.75, 4.25, 5.75, 6.25 (b) x/H= 2.85, 3.35, 3.85, 4.35, 5.75, 6.25

by small-scale turbulent mixing rather than by mixing due to larger-scale meandering. The bipolar nature of the profiles grew stronger towards the downstream direction.

4.2 Contours of Concentration

Fig. 17 shows the instantaneous concentration in the x-y and x-z planes across the center of the nozzle over the smooth and rough beds. Fig. 17(a) and Fig. 17(c) are for the smooth bed. Fig. 17(b) and Fig. 17(d) are for the rough bed. The instantaneous concentration is more elongated and coherent over the smooth bed than that over the rough bed. Scalar is spread quicker but less coherent over the rough bed is visible. It implies an correlation between scalar concentration with coherent structures, for example, streak structures.

The contours of vorticity magnitude and concentration over the smooth bed in x-y plane and x-z plane are depicted separately in Fig. 18. Both x-y plane and x-z plane were through the center of nozzle. The solid lines in Fig. 18 show contours of concentration. As shown in Fig. 18(a), the contours of concentration coincides with those of the vorticity magnitude. Since the vorticity magnitude educes secondary structures and shear layers, it suggests a strong correlation between scalar structures and coherent structures. That is, the vorticity magnitude gradient is high in the locations with high concentration gradient. Fig. 19 shows the contours of vorticity magnitude and concentration over rough bed. The presence of turbulent structures (area of none-zero vorticity) in the entire depth is clear seen from the Fig. 18 and Fig. 19. The vorticity structures shown in the figure reveals the flow separation at the surface of roughness element and recirculation between the cubes. The features

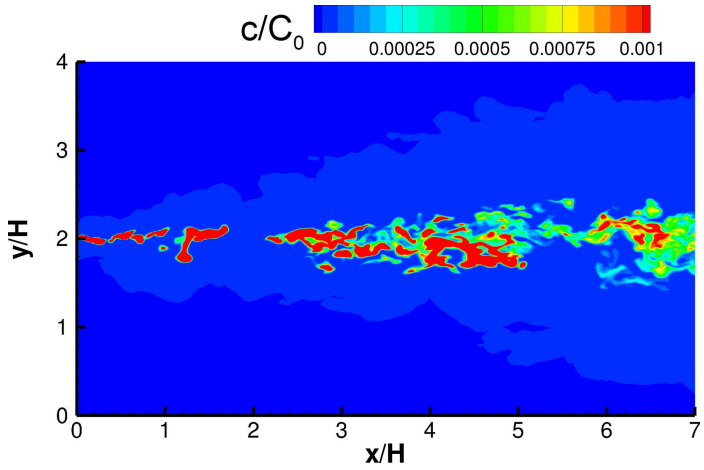

(a)

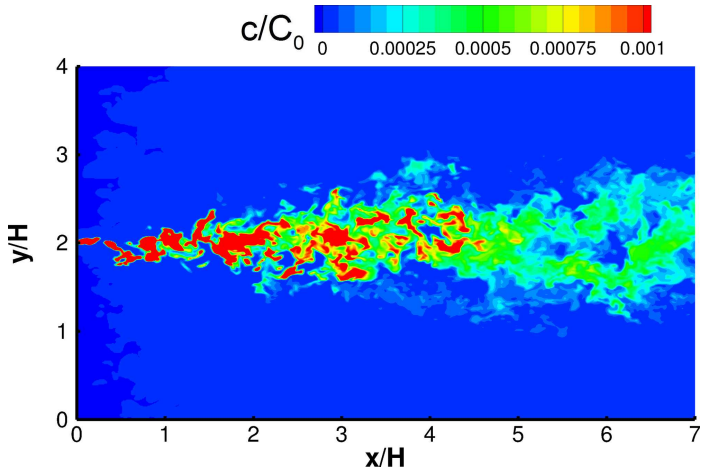

(b)

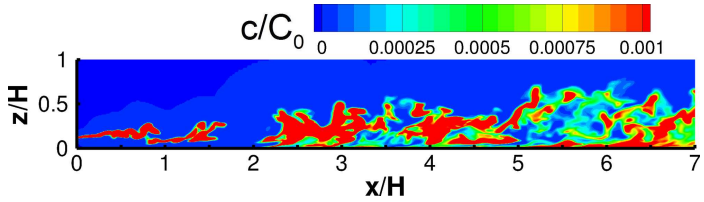

(c)

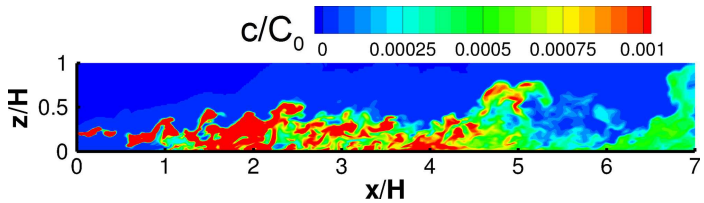

(d)

Figure 17: Contours of instantaneous concentration c/C_0 through the center of nozzle :(a) x-y plane over the smooth bed (b) x-y plane over rough bed (c) x-z plane over the smooth bed (d) x-z plane over rough bed

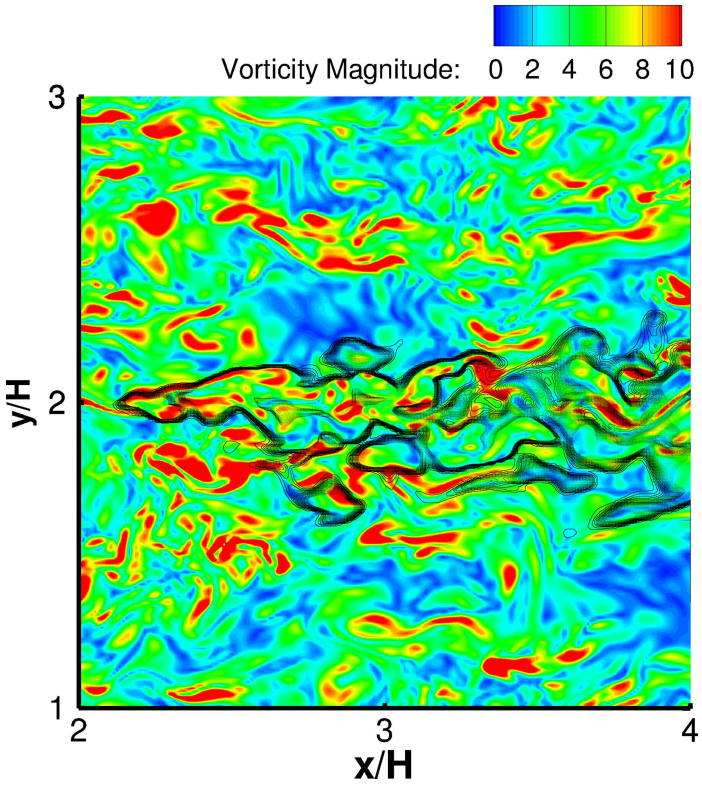

(a)

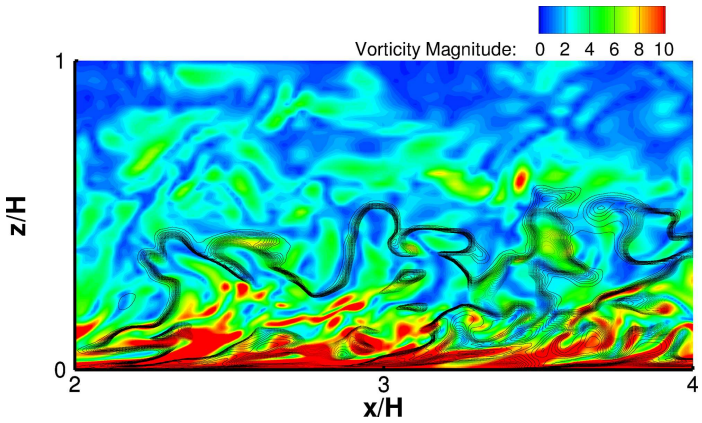

(b)

Figure 18: Contours of vorticity magnitude and concentration with smooth bed: (a) x-y plane (b) x-z plane

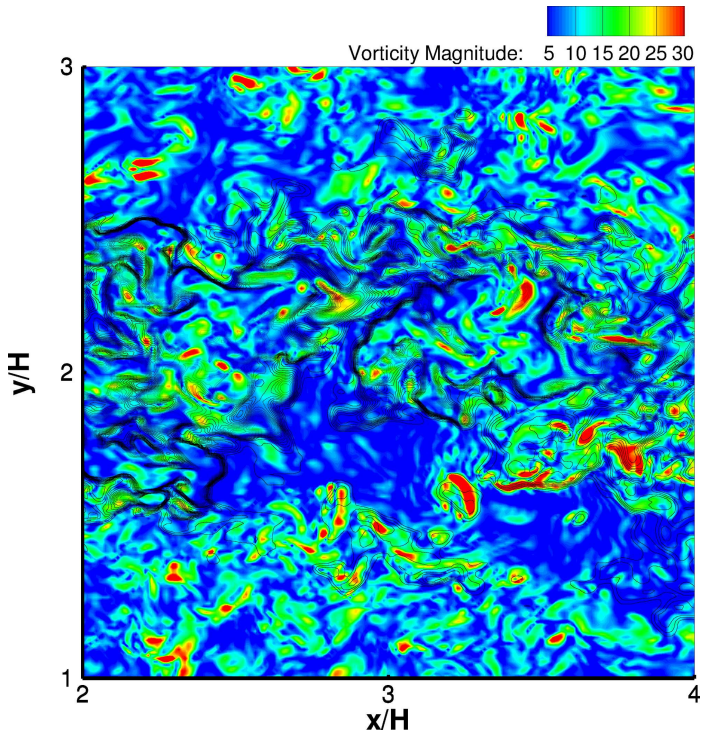

(a)

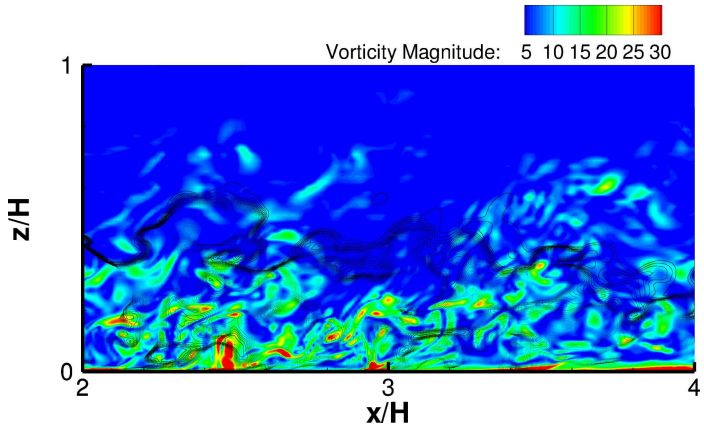

(b)

Figure 19: Contours of vorticity magnitude and concentration with rough bed: (a) x-y plane (b) x-z plane

of flow obtained from LES results, are similar to the ones observed in many of the experimental studies conducted so far.

Areas of high vorticity are plotted with concentration iso-surface to visualize the structures of flow and scalar concentration. The structure of large-scale turbulence is a key mechanism for dynamical process of scalar transfer. Both the scalar and velocity fields were observed to exhibit small-scale(internal) intermittency characterized by strong variability in dissipation and mixing rates (Lesieur and Metais [1996],Warhaft [2000]). Rossi et al. [2010] drew the conclusion that vortical structures do not cause a significant flapping movement of the plume by analyzing the probability density function of concentration at selected points. Orlandi and Leonardi [2004] visualized the passive scalar in a horizontal plane. They observed when the disturbance on the wall was applied, the low and high streaks were not more clearly discernible, while the concentration fluctuations were more isotropic.

4.3 Three-dimensional Concentration Structures

In the study of turbulent flow, the turbulence has quite often been regarded as a random phenomenon. So many researchers studied the turbulent flow by discovering the presence of coherent structures in the flow, which bring some sort of organization to the randomness (Table. 2). In this section, to understand the complex organization and structures in scalar dispersion, comparison between three-dimensional iso-surfaces of scalar concentration and known coherent structures of turbulent flow is presented.

For the identification of the three dimensional vortex structures in the turbulent flow, Jeong and Hussain [1995] suggested a parameter called the 'Q-criterion' to

provide a complete view of the vortex structures. Q is defined as $\frac{1}{2}(||\Omega||^2 - ||S||^2)$, where $||\Omega||$ is the rate of strain tensor and $||S||$ is the vorticity tensor. The three dimensional visualization of the flow is performed by plotting an iso-surface of the Q-criterion and instantaneous concentration.

Fig. 20 and Fig. 21 show three-dimensional views of instantaneous concentration structure together with isosurface of Q of the turbulent flow over the smooth bed and the rough bed respectively. The turbulent nature of the flow comprising of complex three dimensional vortical structures is clearly visible from these figures. The flow over the smooth bed in an open channel is organized in streaks, which forces the scalar contain more in longitudinal. In the rough case, since the flow is of less organization, the scalar in the flow spreads more. It's believed that the observed complex structures are caused by the interaction of hairpin vortices generated from roughness element, shear in the outer layers, and the recirculation in the region between cubes. Fig. 22 and Fig. 23 are snapshots of concentration's and Q-criterion's structures. In Fig. 23, the iso-surfaces of concentration coincided with the hairpin vortices, but the structures were not as distinct as in the smooth case.

Fig. 24 and Fig. 25 show the velocity distribution on the iso-surfaces of concentration at different time instants over the smooth bed and rough bed, respectively. For the smooth case, the iso-surfaces of instantaneous concentration $c/C_0 = 0.0005$ are plotted, and velocity profile is plotted on the iso-surfaces. For the rough case, since the concentration structures are less organized, the iso-surfaces of $c/C_0 = 0.001$ are plotted. The difference between the iso-surface of each neighboring two instants is constant and small.

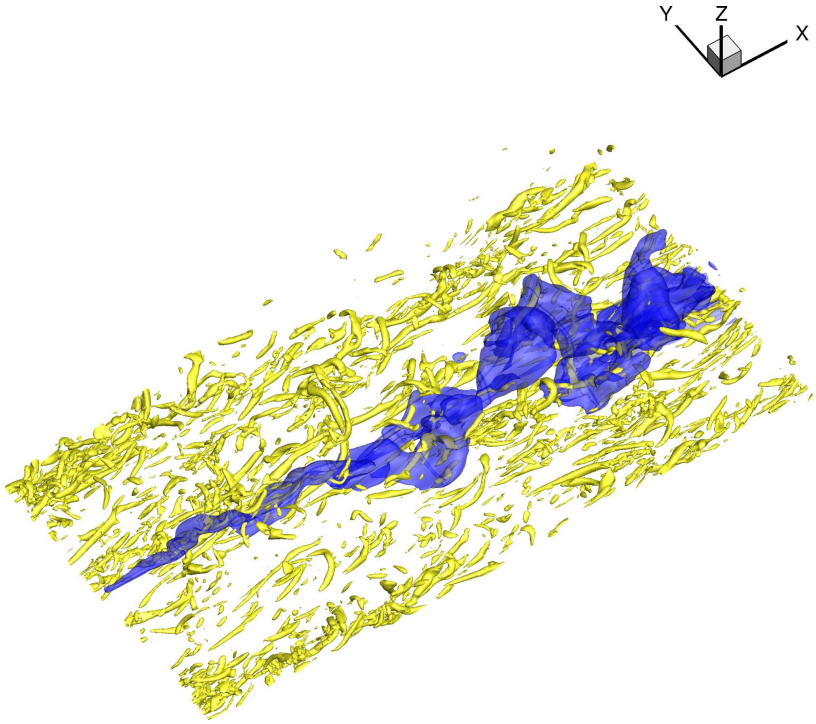

Figure 20: Iso-surfaces of 'Q-criterion' and instantaneous concentration over the smooth bed

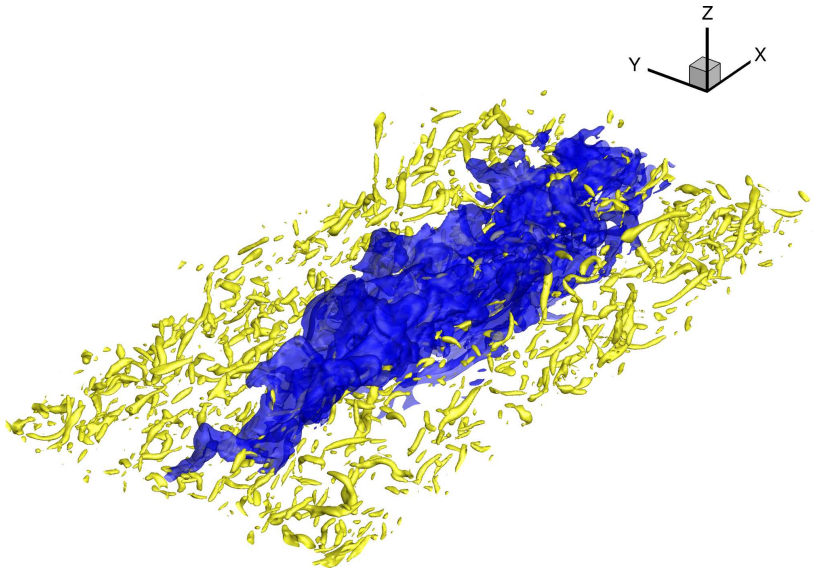

Figure 21: Iso-surface of the 'Q-criterion' and instantaneous concentration over rough bed

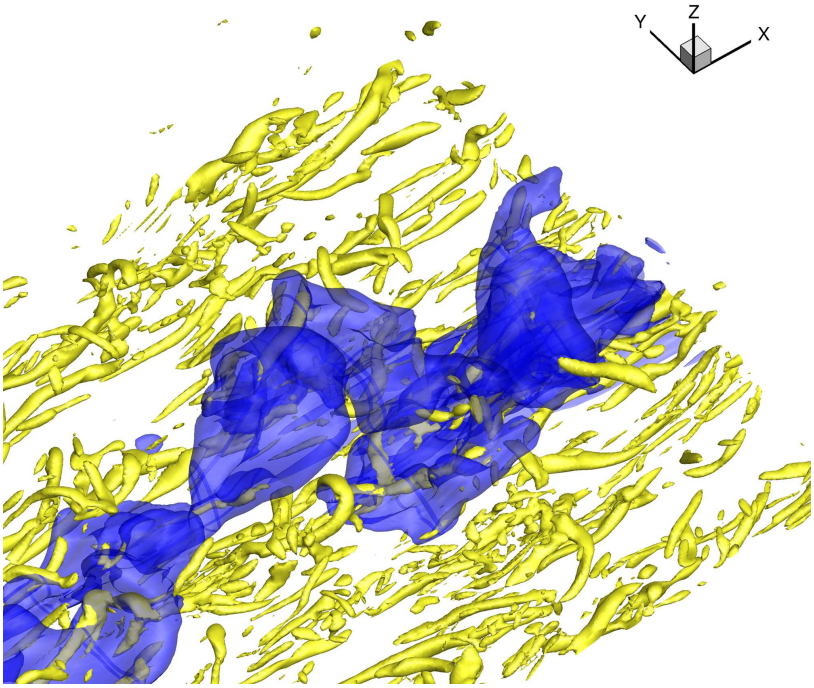

Figure 22: Snapshot of 'Q-criterion' with concentration over the smooth bed

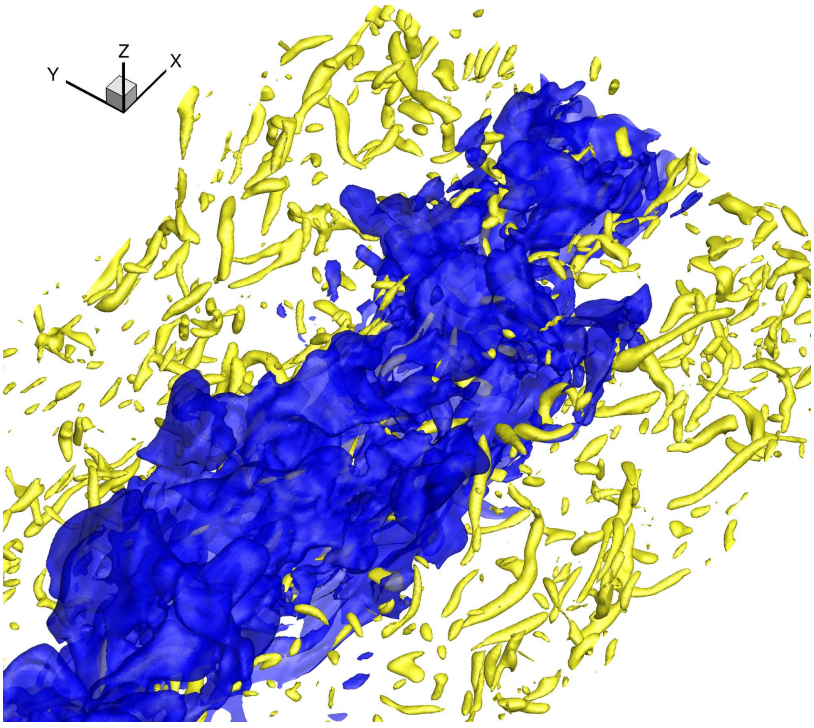

Figure 23: Snapshot of 'Q-criterion' with concentration over rough bed

The generating process of hairpin structure in concentration were present as a series of concentration iso-surfaces. In Panton [2001], they observed that the spanwise vortices developed into a primary hairpin vortex and a "pocket" vortex. The latter vortex was strongly stretched, intensified, and wrapped secondary hairpins from the streaks. Zhou et al. [1996] illustrated the hairpin structures in the vortical structure regenerating process, such as primary hairpin vortex, secondary hairpin vortex, downstream hairpin vortex and quasistreamwise vortices. Similar structures exist in the the iso-surfaces of concentration. From the plots, it is observed that the hairpin tails stretched and moved towards the wall while the heads lifted away. Besides that, the structure of secondary hairpin can be observed in Fig. 24 and Fig. 25.

The three-dimensional views of concentration reveal the existence of hairpin structure in instantaneous concentration. For the smooth case, the iso-surfaces of concentration are organized and self-similar. For the rough case, there are some obvious spatial breaks between the iso-surfaces of concentration, which might be the results of violent ejections from the rough bed.

4.4 Conclusion

In this section, statistical characteristics of scalar, contours of concentration and three-dimensional structures are presented. The statistical characteristics of scalar were in accordance with analytical results and experimental data. The contours of concentration with vorticity magnitude suggested a strong correlation between the scalar dispersion and vorticity field. From the three-dimensional views of concentration iso-surfaces at different instants, the dynamics process of scalar dispersion and

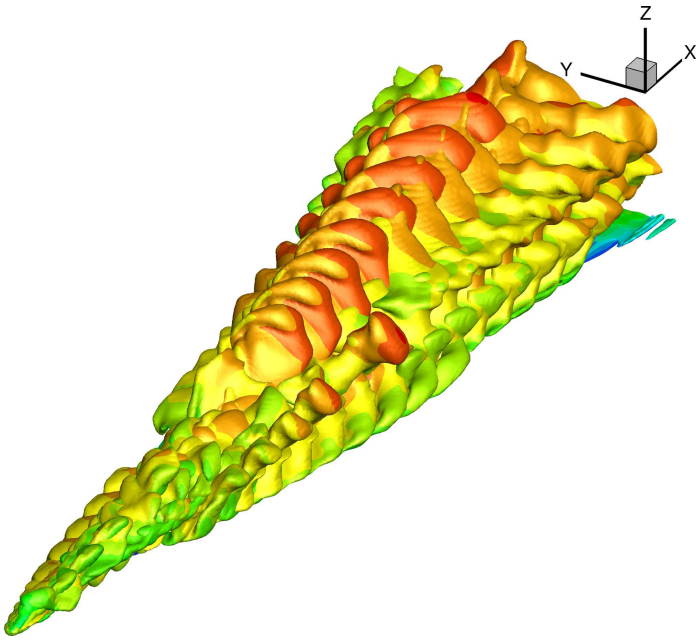

Figure 24: Iso-surfaces of instantaneous concentration at a series of time-steps for smooth bed,$c/C_0 = 0.0005$

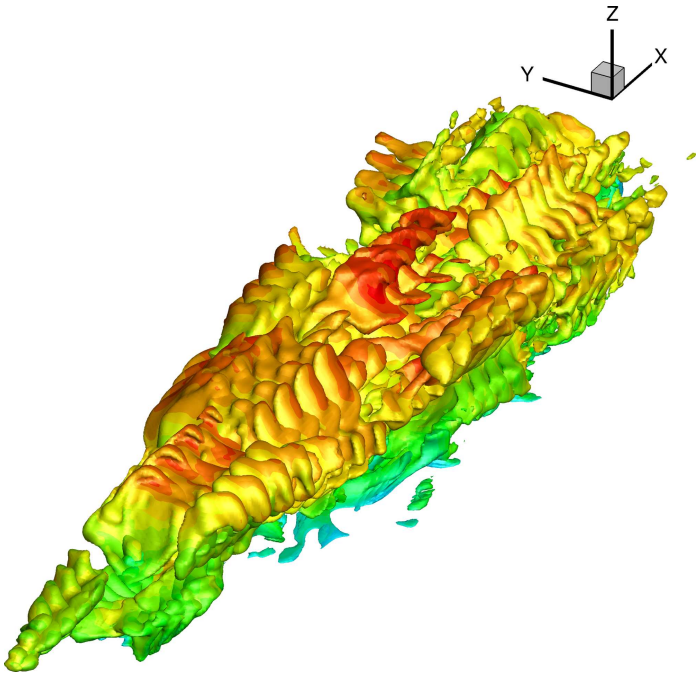

Figure 25: Iso-surfaces of instantaneous concentration at a series of time-steps for rough bed, $c/C_0 = 0.001$

coherent structures of scalar concentration can be exhibited.

CHAPTER V

CONCLUSION

This thesis presented the results of Large Eddy Simulation (LES) of turbulent flow with scalar released in smooth and rough channels. The LES results showed excellent agreement with earlier experimental and numerical studies. The obtained turbulent statistics of velocity field agreed with previous experimental results and theoretical predictions. Also, an increase in roughness Reynolds number (K_s+) led to an increased downshift in mean velocity profiles from the smooth bed profile on a log plot. The averaged concentration on the centerline grew as a power law $c_{y=\bar{0},z=0} \propto x^{-p}$. The comparison of numerical and experimental results showed the differences between the real and the simplified case, which indicated the effects of roughness element geometries. The contours of instantaneous vorticity magnitude and concentration revealed the correlation between concentration structures and coherent turbulent structure in the flow. The hairpin vortices and secondary hairpin structures were observed from the iso-surfaces of concentration. Since the present work provides visualizations of concentration structures with coherent turbulent structures, future efforts should focus on understanding the mechanism of concentration structures generation and the correlations between the concentration and velocity fields.

Although many numerical studies have been performed on this topic, this thesis contributes to the research on scalar dispersion in the following aspects:

(a) The contours of concentration and vorticity magnitude of flow were compared, and suggested a strong correlation between instantaneous scalar concentration and turbulent coherent structures. Coherent structures were identified as ejections, sweeps, hairpin vortex and streaks. In the turbulent channel flow over smooth bed, the scalar was elongated and organized. While in the rough case, the scalar concentration was less coherent due to the violent ejections from cubes.

(b) Iso-surfaces of instantaneous concentration showed that the transport and dispersion is governed by hairpin vortices.

(c) Lateral dispersion is a result of high and low speed streaks, which in the case of a smooth bed are more organized and hence the lateral scalar dispersion is less than over a rough bed.

Bibliography

Armando Babiano and Antonello Provenzale. Coherent vortices and tracer cascades in two-dimensional turbulence. *Journal Of Fluid Mechanics*, 574:429–448, 2007.

J. Bakosi, P. Franzese, and Z. Boybeyi. Probability density function modeling of scalar mixing from concentrated sources in turbulent channel flow. *Physics Of Fluids*, 19(11), 2007.

J. F. Barlow and S. E. Belcher. A wind tunnel model for quantifying fluxes in the urban boundary layer. *Boundary-Layer Meteorology*, 104(1):131–150, 2002.

Se Belcher. Mixing and transport in urban areas. *Philosophical Transactions Of The Royal Society A-Mathematical Physical And Engineering Sciences*, 363(1837):2947–2968, 2005.

K. Bhaganagar, J. Kim, and G. Coleman. Effect of roughness on wall-bounded turbulence. *Flow Turbulence And Combustion*, 72(2-4):463–492, 2004.

S. Bomminayuni and T. Stoesser. Turbulence statistics in an open-channel flow over a rough bed. *Journal Of Hydraulic Engineering-Asce*, 137(11):1347–1358, 2011.

S. Branford, O. Coceal, T. G. Thomas, and S. E. Belcher. Dispersion of a point-source release of a passive scalar through an urban-like array for different wind directions. *Boundary-Layer Meteorology*, 139(3):367–394, 2011.

E. S. C. Ching. Probability densities of turbulent temperature-fluctuations. *Physical Review Letters*, 70(3):283–286, 1993.

J. P. Crimaldi and J. R. Koseff. Structure of turbulent plumes from a momentumless source in a smooth bed. *Environmental Fluid Mechanics*, 6(6):573–592, 2006.

A. Defina. Transverse spacing of low-speed streaks in a channel flow over a rough bed. In P.A. Ashworth, S.J. Bennett, J.L. Best, and S.J. Mclelland, editors, *Coherent Flow Structures In Open Channels*. Wiley, 1996.

Pe Dimotakis. Turbulent mixing. *Annual Review Of Fluid Mechanics*, 37:329–356, 2005.

Hugo B. Fischer, John E. List, C.Robert. Koh, Jorg. Imberger, and Norman H. Brooks. *Mixing In Inland And Coastal Waters*. Academic Press, 1979.

M Germano, U Piomelli, P Moin, and Wh Cabot. A dynamic subgrid-scale eddy viscosity model. *Physics Of Fluids A-Fluid Dynamics*, 3(7):1760–1765, Jul 1991. ISSN 0899-8213. doi: 10.1063/1.857955.

Aj Grass. Structural features of turbulent flow over smooth and rough boundaries. *Journal Of Fluid Mechanics*, 50(Nov29):233, 1971.

Aj. Grass, Rj. Stuart, and M. Mansourtehrani. Vortical structures and coherent motion in turbulent-flow over smooth and rough boundaries. *Philosophical Transactions Of The Royal Society Of London Series A-Mathematical Physical And Engineering Sciences*, 336 (1640):35–65, Jul 15 1991.

V. Haverd, M. Bohm, and M. R. Raupach. The effect of source distribution on bulk scalar transfer between a rough land surface and the atmosphere. *Boundary-Layer Meteorology*, 135(3):351–368, 2010.

Jayesh and Z. Warhaft. Probability-distribution, conditional dissipation, and transport of passive temperature-fluctuations in grid-generated turbulence. *Physics Of Fluids A-Fluid Dynamics*, 4(10):2292–2307, 1992.

J. Jeong and F Hussain. On the identification of a vortex. *Journal Of Fluid Mechanics*, 285:69–94, Feb 25 1995.

N. Kasagi, Y. Tomita, and A. Kuroda. Direct numerical-simulation of passive scalar field in a turbulent channel flow. *Journal Of Heat Transfer-Transactions Of The Asme*, 114 (3):598–606, 1992.

A. R. Kerstein. Linear-eddy modeling of turbulent transport .6. microstructure of diffusive scalar mixing fields. *Journal Of Fluid Mechanics*, 231:361–394, 1991.

Dongjin Kim, Doo-Il Kim, Jae-Hong Kim, and Thorsten Stoesser. Large eddy simulation of flow and tracer transport in multichamber ozone contactors. *JOURNAL OF ENVIRONMENTAL ENGINEERING-ASCE*, 136(1):22–31, JAN 2010.

W. Kollmann and J. Janicka. The probability density-function of a passive scalar in turbulent shear flows. *Physics Of Fluids*, 25(10):1755–1769, 1982.

B. R. Lane, O. N. Mesquita, Sr. Meyers, and J. P. Gollub. Probability-distributions and thermal transport in a turbulent grid flow. *Physics Of Fluids A-Fluid Dynamics*, 5(9): 2255–2263, 1993.

B. E. Launder. *Hear and mass transfer*. Springer, 1978.

S. Leonardi, F. Tessicini, P. Orlandi, and R. Antonia. Direct numerical and large-eddy simulations of turbulent flows over rough surfaces. *Aiaa Journal*, 44(11):2482–2487, 2006.

M Lesieur and O Metais. New trends in large-eddy simulations of turbulence. *Annual Review Of Fluid Mechanics*, 28:45–82, 1996.

D. M. Lu and G. Hetsroni. Direct numerical-simulation of a turbulent open-channel flow with passive heat-transfer. *International Journal Of Heat And Mass Transfer*, 38(17): 3241–&, 1995.

T. Michioka, A. Sato, H. Takimoto, and M. Kanda. Large-eddy simulation for the mechanism of pollutant removal from a two-dimensional street canyon. *Boundary-Layer Meteorology*, 138(2):195–213, 2011.

L. Mydlarski and Z. Warhaft. Passive scalar statistics in high-peclet-number grid turbulence. *Journal Of Fluid Mechanics*, 358:135–175, 1998.

Y. Na and T. J. Hanratty. Limiting behavior of turbulent scaler transport close to a wall. *International Journal Of Heat And Mass Transfer*, 43(10):1749–1758, 2000.

R. Nagaosa. Direct numerical simulation of vortex structures and turbulent scalar transfer across a free surface in a fully developed turbulence. *Physics Of Fluids*, 11(6):1581–1595, 1999.

P. Orlandi and S. Leonardi. Passive scalar in a turbulent channel flow with wall velocity disturbances. *Flow Turbulence And Combustion*, 72(2-4):181–197, 2004.

P. Orlandi and S. Leonardi. Direct numerical simulation of three-dimensional turbulent rough channels: Parameterization and flow physics. *Journal Of Fluid Mechanics*, 606: 399–415, 2008.

M. R. Overholt and S. B. Pope. Direct numerical simulation of a passive scalar with imposed mean gradient in isotropic turbulence. *Physics Of Fluids*, 8(11):3128–3148, 1996.

Rl Panton. Overview of the self-sustaining mechanisms of wall turbulence. *Progress In Aerospace Sciences*, 37(4):341–383, May 2001.

S. B. Pope. Probability approach to modeling of turbulent reacting flows. *Combustion And Flame*, 27(3):299–312, 1976.

S. B. Pope and E. S. C. Ching. Stationary probability density-functions - an exact result. *Physics Of Fluids A-Fluid Dynamics*, 5(7):1529–1531, 1993.

S. Rahman and D. R. Webster. The effect of bed roughness on scalar fluctuations in turbulent boundary layers. *Experiments In Fluids*, 38(3):372–384, 2005.

R. Rossi, D. A. Philips, and G. Iaccarino. A numerical study of scalar dispersion downstream of a wall-mounted cube using direct simulations and algebraic flux models. *International Journal Of Heat And Fluid Flow*, 31(5):805–819, 2010.

Riccardo. Rossi and Gianluca. Iaccarino. Numerical simulation of scalar dispersion downstream of a square obstacle using gradient-transport type models. *Atmospheric Environment*, 43(16):2518–2531, 2009.

B. I. Shraiman and E. D. Siggia. Scalar turbulence. *Nature*, 405(6787):639–646, 2000.

Y. G. Sinai and V. Yakhot. Limiting probability-distributions of a passive scalar in a random velocity-field. *Physical Review Letters*, 63(18):1962–1964, 1989.

K. R. Sreenivasan. The passive scalar spectrum and the obukhov-corrsin constant. *Physics Of Fluids*, 8(1):189–196, 1996.

I. Tiselj, E. Pogrebnyak, C. Li, A. Mosyak, and G. Hetsroni. Effect of wall boundary condition on scalar transfer in a fully developed turbulent flume. *Physics Of Fluids*, 13 (4):1028–1039, 2001.

A. Walton and A. Y. S. Cheng. Large-eddy simulation of pollution dispersion in an urban street canyon - part ii: Idealised canyon simulation. *Atmospheric Environment*, 36(22): 3615–3627, 2002.

B. C. Wang, E. Yee, and F. S. Lien. Numerical study of dispersing pollutant clouds in a built-up environment. *International Journal Of Heat And Fluid Flow*, 30(1):3–19, 2009.

Z. Warhaft. Passive scalars in turbulent flows. *Annual Review Of Fluid Mechanics*, 32: 203–240, 2000.

Z. T. Xie, P. Hayden, A. G. Robins, and P. R. Voke. Modelling extreme concentrations from a source in a turbulent flow over a rough wall. *Atmospheric Environment*, 41(16): 3395–3406, 2007.

E Yee, Dj Wilson, and Bw Zelt. Probability-distributions of concentration fluctuations of a weakly diffusive passive plume in a turbulent boundary-layer. *Boundary-Layer Meteorology*, 64(4):321–354, Jun 1993.

A. Yoshizawa. Statistical modeling of passive-scalar diffusion in turbulent shear flows. *Journal Of Fluid Mechanics*, 195:541–555, 1988.

Jg. Zhou, Rj. Adrian, and S Balachandar. Autogeneration of near-wall vortical structures in channel flow. *Physics Of Fluids*, 8(1):288–290, Jan 1996.

Y. Zhu, R. A. Antonia, and I. Hosokawa. Refined similarity hypotheses for turbulent velocity and temperature-fields. *Physics Of Fluids*, 7(7):1637–1648, 1995.